JUSTC

Article

http://justc.ustc.edu.cn

Received: April 06, 2022; Accepted: May 06, 2022

Boosting photocatalytic Suzuki coupling reaction over Pd nanoparticles by regulating Pd/MOF interfacial electron transfer

Zi-Xuan Sun, and Hai-Long Jiang ✉

Department of Chemistry, University of Science and Technology of China, Hefei 230026, China

✉Correspondence: Hai-Long Jiang, E-mail: jianglab@ustc.edu.cn

Graphical abstract

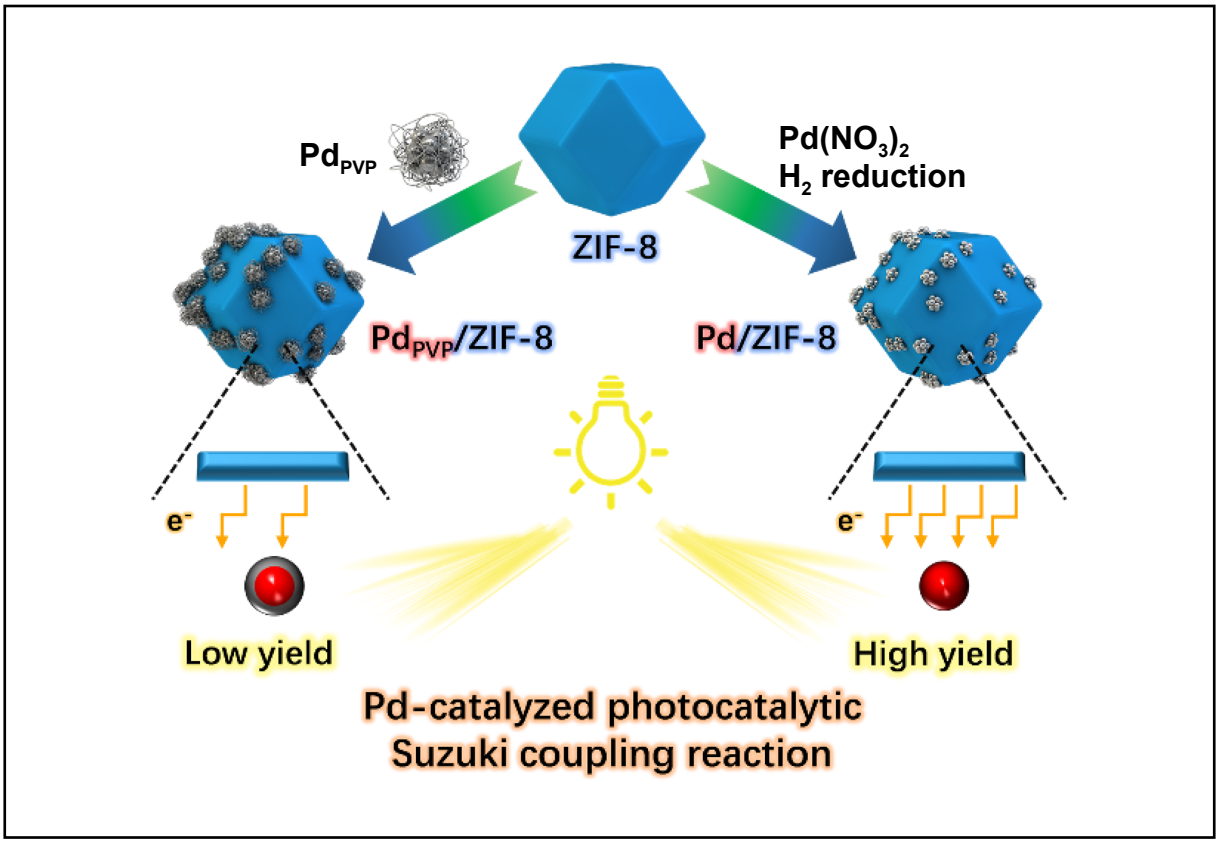

Interfacial electron transfer determines the Pd photocatalytic activity in Pd/ZIF-8.

Public summary

- Pd_{PVP}/ZIF-8 and Pd/ZIF-8 were precisely synthesized with similar Pd sizes and loadings, providing models for investigating the metal-support interfacial effect.
- A photocatalytic Suzuki coupling reaction was performed with Pd_{PVP}/ZIF-8 (57.9% yield) and Pd/ZIF-8 (99.1% yield) in 5 h, showing the advantages of Pd/ZIF-8 without surfactants in the Pd-MOF interface.
- Control experiments and characterizations confirmed the photocatalytic mechanism and further concluded that Pd/ZIF-8 had better interfacial electron transfer than that of Pd_{PVP}/ZIF-8.

Citation: Sun Z-X, Jiang H-L. Boosting photocatalytic Suzuki coupling reaction over Pd nanoparticles by regulating Pd/MOF interfacial electron transfer. *JUSTC*, **2022**, 52(8): 5. DOI: 10.52396/JUSTC-2022-0063

JUSTC

Article

http://justc.ustc.edu.cn

Received: April 06, 2022; Accepted: May 06, 2022

Boosting photocatalytic Suzuki coupling reaction over Pd nanoparticles by regulating Pd/MOF interfacial electron transfer

Zi-Xuan Sun, and Hai-Long Jiang ✉

Department of Chemistry, University of Science and Technology of China, Hefei 230026, China

✉Correspondence: Hai-Long Jiang, E-mail: jianglab@ustc.edu.cn

Cite This: *JUSTC*, **2022**, 52(8): 5 (7pp)

Read Online

Abstract: Palladium-catalyzed C-C coupling reactions are of significant importance, but they often require harsh conditions. Herein, we report an interface-regulated photocatalytic Suzuki coupling reaction over Pd nanoparticles supported on a metal-organic framework (MOF), ZIF-8. Two Pd/MOFs were synthesized, Pd_{PVP}/ZIF-8 and Pd/ZIF-8, which have similar Pd sizes and loading amounts, except that the former contains poly(vinylpyrrolidone) (PVP) as a surfactant. The diffuse-reflectance infrared Fourier transform of CO adsorption (CO-DRIFT) indicates that Pd/ZIF-8 represents a more negative electronic state of Pd than Pd_{PVP}/ZIF-8. In the photocatalytic Suzuki coupling reaction between iodobenzene and phenylboronic acid, Pd/ZIF-8 exhibits excellent performance (99.1% yield), much better than that of Pd_{PVP}/ZIF-8 (57.9% yield). Moreover, Pd/ZIF-8 is highly stable and shows broad substrate scope for this reaction. The superior activity of Pd/ZIF-8 can be attributed to sufficient electron transfer between the MOFs and Pd nanoparticles in the absence of an interfacial surfactant. This work provides new insights into a Pd-catalyzed C-C coupling reaction involving photocatalysis and interfacial electron transfer.

Keywords: metal-organic framework; Pd nanoparticles; Suzuki coupling; electron transfer; photocatalysis

CLC number: O643.3 **Document code:** A

1 Introduction

The palladium (Pd)-catalyzed Suzuki cross-coupling reaction has been one of the most effective methods for the one-step formation of carbon-carbon bonds since its discovery in 1979[1, 2]. Typical Pd catalysts are homogeneous Pd complexes because they have high catalytic efficiency[3]. However, their high price and the difficulty of recycling hinders their industrial application. Pd nanoparticles can be substituted for the Pd complexes in this reaction, but the reaction requires a high temperature to provide the necessary activation energy, leading to undesirable side reactions and reduced catalyst stability[4]. A photocatalytic Suzuki coupling reaction using interband excitation of Pd nanoparticles has recently been reported[5]. This approach has the advantage of utilizing sustainable solar energy and relatively mild conditions, but it is still limited by a low reaction rate. It is therefore imperative to develop methods to optimize the photocatalytic Suzuki coupling of Pd nanoparticles.

It is well known that because metal nanoparticles have high surface energy they tend to aggregate and lose their activity. To address this issue, different support materials have been used to stabilize the nanoparticles, such as metal oxides [6], zeolites[7], and carbon materials[8]. The contact between the support matrix and the metal nanoparticles gives rise to a metal-support interaction (MSI)[9], which has a powerful influence on the catalytic performance of the metal nanoparticles. Such metal-support interactions include morphology and size effects[10], interfacial effects[11], electron transfer[12], and strong metal-support interactions[13]. Among these, modulating the interfacial effect and electron transfer process is a direct and effective way to influence the catalytic properties of metal nanoparticles. Considering that the photocatalytic reactions of Pd nanoparticles involve electron transfer to or from Pd[5], it is promising to regulate the reaction rate via interfacial electron transfer between the support and the Pd nanoparticles.

Metal-organic frameworks (MOFs), composed of metal (clusters) and organic linkers, have the properties of high crystallinity, porosity, and designability, and have attracted much attention in recent years[14–16]. MOFs are excellent supports for metal nanoparticles because they possess large surface areas to stabilize the nanoparticles and can regulate their electronic states [17, 18]. Moreover, MOFs are semiconductor-like and can form Schottky contacts with metal nanoparticles, facilitating electron transfer between MOFs and metal nanoparticles[19, 20]. Interfacial electron transfer between MOFs and metal nanoparticles has been reported recently[21], which inspired our design to boost Pd-catalyzed photocatalytic reactions by regulating the interface between MOFs and Pd nanoparticles.

In this study, we synthesized two catalysts with different interfaces between an MOF (the zeolitic imidazolate framework ZIF-8) and Pd nanoparticles. Pd/ZIF-8 was synthesized by an impregnation method and its interface is “clean”, whereas Pd_{PVP}/ZIF-8 was obtained by mixing ZIF-8 with pre-synthesized Pd_{PVP} nanoparticles, and its interface contains poly (vinylpyrrolidone) (PVP) as a barrier. Although these two

DOI: 10.52396/JUSTC-2022-0063

JUSTC, **2022**, 52(8): 5

catalysts have the same MOF support and similar Pd sizes and loadings, their Pd electronic states are distinct, giving rise to a higher photocatalytic activity of Pd/ZIF-8 in the Suzuki coupling reaction compared to Pd_{PVP}/ZIF-8. From analysis of the photocatalytic mechanism, we conclude that the superior interfacial electron transfer in Pd/ZIF-8 is responsible for its improved activity. This work provides inspiration for the study of Pd-catalyzed Suzuki coupling reactions from the perspective of regulating interfacial electron transfer.

2 Results and discussion

2.1 Preparation and characterization of catalysts

The representative stable MOF, ZIF-8, formulated Zn(2-MIM)$_2$ (2-MIM represents 2-methylimidazole), was chosen as the support for Pd nanoparticles and was synthesized by the solvothermal method[22, 23]. Comparison of the powder X-ray diffraction (XRD) pattern of as-synthesized ZIF-8 with a simulated XRD pattern of ZIF-8 indicates that the ZIF-8 obtained was a pure phase with high crystallinity (Fig. 1a). Scanning electron microscopy (SEM) images showed that the ZIF-8 nanocrystals had a rhombic dodecahedron shape and a mean size of ~1 μm (Fig. 1b). To prepare Pd_{PVP}/ZIF-8, we first synthesized Pd_{PVP} nanoparticles following a reported method[24]. Transmission electron microscopy (TEM) showed that the size distribution of Pd_{PVP} nanoparticles was from 2.8 to 4.5 nm with an average size of ~3.68 nm (Fig. 1c). Pd_{PVP}/ZIF-8 was obtained by stirring mixed dispersions of ZIF-8 and pre-synthesized Pd_{PVP} nanoparticles, whereas Pd/ZIF-8 was synthesized by impregnation of ZIF-8 with $Pd(NO_3)_2$ in aqueous solution, followed by reduction by H_2. TEM images confirmed the successful introduction of Pd nanoparticles onto the ZIF-8 support by both methods, the sizes of the obtained Pd nanoparticles being quite similar (~3.68 nm for Pd_{PVP}/ZIF-8 and ~3.92 nm for Pd/ZIF-8) (Fig. 1d ,e). Inductively coupled plasma atomic emission spectrometry (ICP-AES) indicated similar Pd loadings for the two catalysts (2.01 wt% for Pd_{PVP}/ZIF-8 and 1.98 wt% for Pd/ZIF-8) (Table 1).

The integrity of ZIF-8 after post-modification was first confirmed by powder XRD patterns, which indicated that Pd_{PVP}/ZIF-8 and Pd/ZIF-8 had good crystallinity, and no obvious peak assignable to Pd was found, indicating the small size of any Pd nanoparticles (Fig. 1a). Comparison of the infrared (IR) spectra of Pd_{PVP}/ZIF-8 and Pd/ZIF-8 with that of ZIF-8 (Fig. 1f) further supported the chemical structures. Nitrogen (N_2) sorption curves at 77 K (Fig. 2a) showed that Pd_{PVP}/ZIF-8 and Pd/ZIF-8 exhibited similar pore structures to the parent ZIF-8, while the slightly decreased BET surface area might be due to the mass occupied by Pd nanoparticles. To confirm the feasibility of the two catalysts for photocatalytic reactions, UV-vis spectra were obtained (Fig. 2b), and indicate that ZIF-8 has no light absorption in the visible light region (380–800 nm), and that both Pd_{PVP}/ZIF-8 and Pd/ZIF-8 nanoparticles have the ability to absorb visible light as a result of interband excitation of Pd nanoparticles [5].

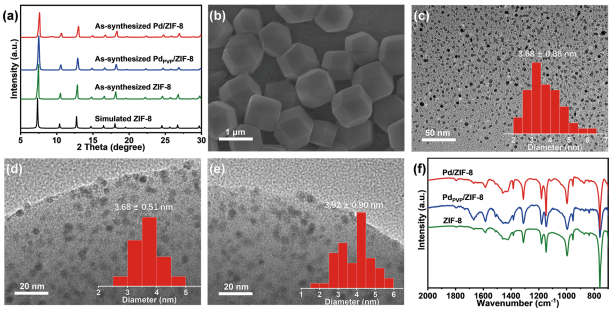

Fig. 1. (a) Powder XRD patterns of simulated ZIF-8 and as-synthesized ZIF-8, Pd_{PVP}/ZIF-8, and Pd/ZIF-8. (b) SEM image of ZIF-8. (c–e) TEM images for (c) Pd_{PVP} nanoparticles, (d) Pd_{PVP}/ZIF-8, and (e) Pd/ZIF-8 . Insets are the size distributions of Pd nanoparticles. (f) IR spectra of ZIF-8, Pd_{PVP}/ZIF-8, and Pd/ZIF-8.

Table 1. The measured Pd loadings for different catalysts.

Catalyst	Content[a]
Pd_{PVP}/ZIF-8	2.01 wt%
Pd/ZIF-8	1.98 wt%
Pd_{PVP}/ZIF-8 after reaction	1.99 wt%
Pd/ZIF-8 after reaction	1.96 wt%

[Note] [a] The Pd contents were confirmed by ICP-AES data.

Mott-Schottky plots (Fig. 2c) were obtained to analyze the semiconductor-like character of ZIF-8. The plots at 500, 1000, and 1500 Hz all have positive slopes, indicating n-type semiconductor character for ZIF-8[25]. Considering that semiconductors and metal nanoparticles form Schottky junctions upon contact and adjust the electronic states of metal nanoparticles[26], we used the diffuse-reflectance infrared Fourier transform of adsorbed CO (CO-DRIFT) to determine the electronic states of the Pd nanoparticles of different catalysts (Fig. 2d). Both Pd_{PVP}/ZIF-8 and Pd/ZIF-8 exhibited the coexistence of two-fold (typically 1 800–2 000 cm^{-1}) and three-fold (typically 1 600–1 800 cm^{-1}) absorption peaks of adsorbed CO molecules, confirming that the Pd species was present in the nanoparticles. Because a more negative electronic state of the metal gives rise to a stronger electron back-donation effect between the metal and adsorbed CO, leading to a red shift of the CO absorption peaks, the positions of these peaks can clearly elucidate the electronic state of the metal[27]. The red shift of the C–O stretching band (typically 2 000–2100 cm^{-1}) of Pd/ZIF-8

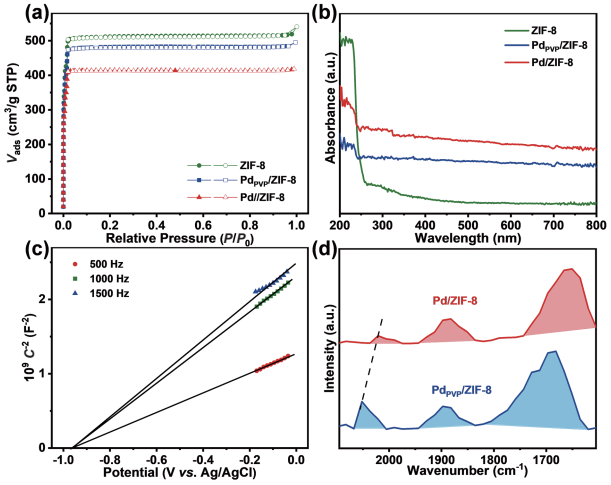

Fig. 2. (a) N_2 sorption curves and (b) UV-vis spectra for ZIF-8, Pd_{PVP}/ZIF-8, and Pd/ZIF-8. (c) Mott-Schottky plots for ZIF-8. (d) DRIFT spectra of CO adsorbed on Pd for Pd_{PVP}/ZIF-8 and Pd/ZIF-8.

DOI: 10.52396/JUSTC-2022-0063
JUSTC, **2022**, 52(8): 5

compared with that of Pd_{PVP}/ZIF-8 indicates that Pd/ZIF-8 has a more negative electronic state, which might be attributed to the different interfaces of the two nanoparticles, and might have influenced their photocatalytic performances.

2.2 Photocatalytic reaction

The Pd_{PVP}/ZIF-8 and Pd/ZIF-8 catalysts were adapted for the photocatalytic Suzuki coupling reaction by using 450 nm LED light irradiation under a N_2 atmosphere. The substrates used were iodobenzene and excess phenylboronic acid, and K_2CO_3 was added to provide an alkaline environment. The conversion and yield were determined by gas chromatography (GC). In a reaction time of 5 h, Pd/ZIF-8 exhibited high activity, with a 99.1% yield of biphenyl; in contrast, Pd_{PVP}/ZIF-8 gave only a 57.8% yield of the target product (Fig. 3a). The stability of the catalysts was first tested by recycling experiments. In three consecutive runs, both catalysts maintained their activity, providing similar conversions and yields to those in their first runs (Fig. 3b,c). The recycled catalysts were examined by powder XRD, TEM, and ICP-AES. Powder XRD showed that the catalysts retained their high crystallinity after the photocatalytic reaction (Fig. 3d). TEM images showed that the aggregation of Pd nanoparticles does not occur in either catalyst (Fig. 3e,f). ICP-AES confirmed that there was almost no mass loss of Pd (Table 1), reflecting the advantages of the MOF supports under mild photocatalytic conditions.

Next, we examined the substrate scope of the best-performing Pd/ZIF-8 catalysts (Table 2). First, when iodobenzene was replaced with bromobenzene, the yield decreased significantly (entry 1), and when chlorobenzene was used as the substrate, almost no product was detected (entry 2). These results can be attributed to the difficulty in reducing C–Br and C–Cl bonds. Therefore, we focused on coupling between iodobenzenes and phenylboronic acid. Three functionalized iodobenzene derivatives (4-iodotoluene, 3-iodotoluene, and 4-iodobenzotrifluoride) showed satisfactory conversion in C-C coupling (entries 3–5; the higher yield from 4-iodotoluene than from 3-iodotoluene might be due to steric and electronic effects). In place of phenylboronic acid, 4-methylphenylboronic acid also participated in the reaction with good conversion (entry 6). The tolerance of different iodobenzene and phenylboronic acid derivatives demonstrated the great practicability

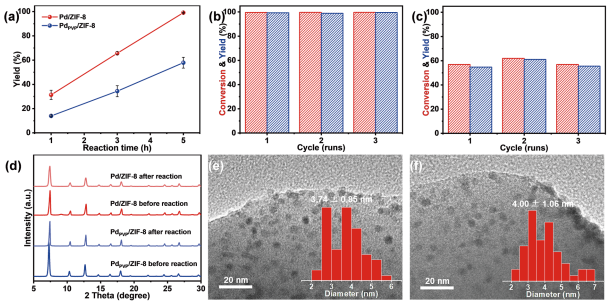

Fig. 3. (a) Time-dependent yields of biphenyl in reactions of Pd_{PVP}/ZIF-8 and Pd/ZIF-8 (the error bars represent the relative deviation obtained from parallel experiments). (b, c) Recycling performance of (b) Pd/ZIF-8 and (c) Pd_{PVP}/ZIF-8. (d) Comparison of powder XRD patterns of Pd_{PVP}/ZIF-8 and Pd/ZIF-8 before and after reaction. (e, f) TEM images of (e) Pd_{PVP}/ZIF-8 and (f) Pd/ZIF-8 after reaction (inset: size distribution of Pd nanoparticles).

Table 2. Results of substrate scope experiments catalazed by Pd/ZIF-8[a].

Entry	Substrate 1	Substrate 2	Conversion of 1 (%)	Yield (%)
1	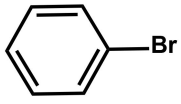	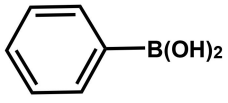	38.60	38.42
2	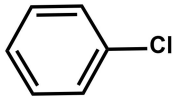	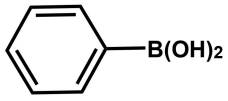	0.06	0.06
3		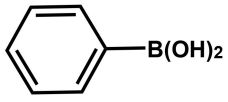	99.99	99.92
4	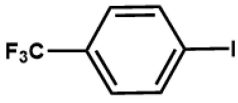	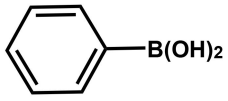	99.99	99.25
5	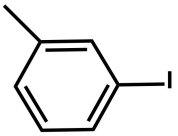	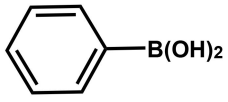	96.52	96.13
6	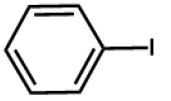	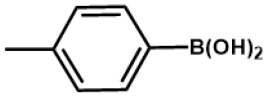	99.85	99.69

[Note] [a] Standard conditions: typically, 10 mg catalyst, 80 mg K_2CO_3, 10 μL iodobenzene (0.1 mmol), 24 mg phenylboronic acid (0.2 mmol) and 2 mL DMF/water (1/1, v/v), LED lamp (450 nm, 80 W), 5 h. The conversion and yield were determined by GC analysis, and *n*-dodecane was used as the internal standard.

DOI: 10.52396/JUSTC-2022-0063
JUSTC, **2022**, 52(8): 5

of our Pd/ZIF-8 photocatalyst.

2.3 Discussion of the differences in activity

Control experiments were performed to elucidate the mechanism of the photocatalytic reaction (Table 3). When no K_2CO_3 was used, the reaction hardly proceeded, indicating that a base played an important role in the reaction process (entry 1). When the light irradiation was replaced by thermal heating, the conversion was low at both 25 ℃ and 60 ℃, probably because of the high activation energy for this reaction via the thermal conversion pathway (entries 2 and 3). Only by elevating the heating temperature to 85 °C can the reaction over Pd/ZIF-8 achieve a similar conversion (100%) to that obtained by photocatalysis. However, the selectivity (71.2%) was lower than that of photocatalysis, and the conversion decreased significantly (to 42.5%) during the recycling experiments. These results clearly demonstrate that the photocatalytic process promotes the reaction under mild conditions. Furthermore, when we replaced the N_2 atmosphere with O_2, no products were detected (entry 4). It is assumed that O_2 is prone to be reduced by accepting electrons to produce superoxide radicals ($O_2^{\cdot-}$) [28], and this impedes the reduction of the substrate, accounting for the failure to detect products.

Scavengers were used to explore the photocatalytic mechanism (Table 3). When *p*-benzoquinone (*p*BQ) was introduced as a typical radical scavenger[29], the conversion was reduced to some extent (entry 5), revealing that radicals are involved in the catalytic process. On the addition of methanol (MeOH), which is readily oxidized by photogenerated hot holes, decreased conversion was observed (entry 6), indicating that hot holes participate in the reaction. Finally, we changed the catalyst to ZIF-8 and a physical mixture of ZIF-8 and Pd_{PVP} nanoparticles; ZIF-8 exhibited no activity and the physical mixture produced only slight conversion (entries 7 and 8), indicating that Pd nanoparticles are indispensable for the photocatalytic process, and the integration of Pd nanoparticles and the ZIF-8 support is beneficial to the reaction.

It is important to determine whether the mechanism is based on photoexcited carriers or on a photothermal effect. We investigated the relationship between the photocatalytic performance of Pd/ZIF-8 and the light intensity. As shown in Fig. 4a, the yield of product has a linear relationship with the light intensity, which excludes the possibility of photothermal catalysis[30]. Based on these results, we proposed a possible reaction mechanism (Fig. 4b). First, under 450 nm light irradiation, Pd nanoparticles undergo interband excitation to form photogenerated hot electrons and holes. The hot electrons then attack the C–I bond, facilitating its cleavage[31]. The hot holes attack the C–B bond of the electronically negative phenyltrihydroxyborate species, which is generated by phenylboronic acid reacting with OH^- in the basic medium. This leads to the formation of a phenyl radical cation[32]. Finally, the phenyl radical cation and activated iodobenzene are coupled on the Pd nanoparticles, followed by reductive elimination to afford biphenyl[33].

To analyze the difference in activity between Pd_{PVP}/ZIF-8 and Pd/ZIF-8, we obtained the photoluminescence (PL) spectra of ZIF-8, Pd_{PVP}/ZIF-8, and Pd/ZIF-8 (Fig. 5a). The intensity of the PL spectra reflects the efficiency of electron-hole separation in ZIF-8. Both Pd_{PVP}/ZIF-8 and Pd/ZIF-8 demonstrated reduced PL intensities compared to ZIF-8, indicating that the Schottky junction between ZIF-8 and Pd nanoparticles results in accelerated electron injection from ZIF-8 into Pd nanoparticles under the test conditions (excitation wavelength 225 nm). Moreover, the decrease in the PL intensity from ZIF-8 to Pd/ZIF-8 was greater than that from Pd_{PVP}/ZIF-8 to Pd/ZIF-8, indicating that the Pd/ZIF-8 interface is more suitable for electron transfer. Combining the distinct Pd electronic states (Fig. 2b), we propose that the difference in photocatalytic activity can be attributed to interfacial electron transfer from ZIF-8 to Pd (Fig. 5b). Upon contact with the ZIF-8 and Pd nanoparticles, the n-type semiconductor-like ZIF-8 transfers electrons to Pd to align the Fermi levels[34]. However, the interfacial surfactant PVP present in Pd_{PVP}/ZIF-8 might act to some extent as a barrier to block electron transfer, reducing the electron density of the Pd nanoparticles. Correspondingly, the higher electron density of the Pd in Pd/ZIF-8 is advantageous for substrate adsorption and activation in the photocatalysts, leading to the higher activity of Pd/ZIF-8 than that of Pd_{PVP}/ZIF-8.

Table 3. Results of substrate scope experiments catalazed by Pd/ZIF-8[a].

Entry	Catalyst	Base	Light	Atmosphere	Additive	Temperature (°C)	Yield (%)
1	Pd/ZIF-8	−	+	N_2	−	25	n.d.
2	Pd/ZIF-8	+	−	N_2	−	25	n.d.
3	Pd/ZIF-8	+	−	N_2	−	60	34.32
4	Pd/ZIF-8	+	+	O_2	−	25	n.d.
5	Pd/ZIF-8	+	+	N_2	*p*BQ	25	70.56
6	Pd/ZIF-8	+	+	N_2	MeOH	25	67.15
7	ZIF-8	+	+	N_2	−	25	n.d.
8[b]	Pd_{PVP}+ ZIF-8	+	+	N_2	−	25	38.42

[Note] [a] Standard conditions: typically, 10 mg catalyst, 80 mg K_2CO_3, 10 μL iodobenzene (0.1 mmol), 24 mg phenylboronic acid (0.2 mmol) and 2 mL DMF/water (1/1, v/v), LED lamp (450 nm, 80 W), 5 h. The conversion and yield were determined by GC analysis, and *n*-dodecane was used as the internal standard.

[b] 100 μL Pd_{PVP} aqueous solution and 10 mg ZIF-8 were added to 1mL of DMF and 0.9 mL deionized water while the other experimental parameters were maintained constant.

DOI: 10.52396/JUSTC-2022-0063
JUSTC, **2022**, 52(8): 5

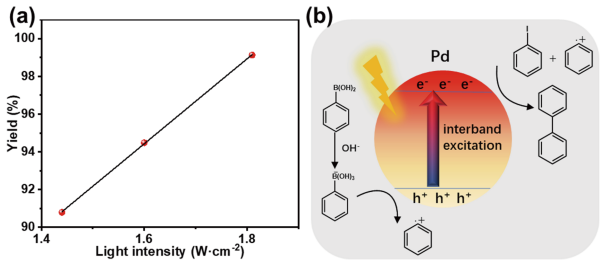

Fig. 4. (a) Relationship between yield and light intensity catalyzed by Pd/ZIF-8. (b) Proposed photocatalytic reaction mechanism.

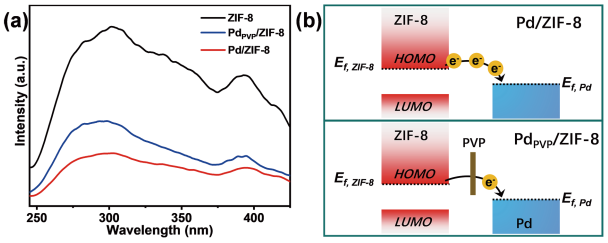

Fig. 5. (a) PL spectra of ZIF-8, Pd_{PVP}/ZIF-8, and Pd/ZIF-8. (b) Interfacial electron transfer between ZIF-8 and Pd nanoparticles.

3 Experimental details

3.1 Materials and instruments

All the chemicals were purchased without further treatment. 2-methylimidazole (2-MIM, 98%, Macklin), zinc acetate dihydrate ($Zn(CH_3COO)_2{\cdot}2H_2O$, AR, Sinopharm Chemical Reagent Co., Ltd.), poly (vinylpyrrolidone) (PVP, M_w = 5 5000, Aldrich Chemistry), *n*-dodecane (AR, Sinopharm Chemical Reagent Co., Ltd.), *p*-benzoquinone (*p*BQ, 98%, Energy Chemical), N,N-dimethylformamide (DMF, AR, Sinopharm Chemical Reagent Co., Ltd.), methanol (MeOH, AR, Sinopharm Chemical Reagent Co., Ltd.), acetone (AR, Sinopharm Chemical Reagent Co., Ltd.), ascorbic acid (AR, Sinopharm Chemical Reagent Co., Ltd.), potassium bromide (KBr, AR, Sinopharm Chemical Reagent Co., Ltd.), potassium chloropalladite (K_2PdCl_4, Shanxi Kaida), $Pd(NO_3)_2$ aqueous solution (50 mg Pd per mL, Sinopharm Chemical Reagent Co., Ltd.), iodobenzene (98%, Energy Chemical), bromobenzene (99.5%, Energy Chemical), chlorobenzene (98%, Energy Chemical), phenylboronic acid (98%, Energy Chemical), 4-iodotoluene (98%, Energy Chemical), 3-iodotoluene (98%, Energy Chemical), 4-iodobenzotrifluoride (98%, bidepharm), 4-tolylboronic acid (98%, Energy Chemical), Nafion dispersion (5% w/w in water and 1-propanol, ≥ 0.92 meq/g exchange capacity, Alfa Aesar). Deionized water (18.25 MΩ·cm) was obtained by reverse osmosis, followed by ion-exchange and filtration (Cleaned Water Treatment Co., Ltd., Hefei).

Powder X-ray diffraction (XRD) patterns were obtained using a Japan Rigaku MiniFlex 600 equipped with graphite-monochromatized Cu Kα radiation (λ = 1.541 78 Å). Scanning electron microscopy (SEM) images were obtained using a Carl Zeiss Supra 40 scanning electron microscope. Transmission electron microscopy (TEM) images were obtained using a field-emission transmission electron microscope (JEOL JEM2100F). Nitrogen sorption measurements were conducted on a Micromeritics ASAP 2020 system at 77 K. UV-vis spectra of the catalysts were obtained using a Shimadzu UV-2700. The Pd content of the catalysts was determined using an Optima 7300 DV inductively coupled plasma atomic emission spectrometer (ICP-AES). Conversions and yields of the corresponding reactions were determined by gas chromatography (GC, Shimadzu 2010 Plus with a 0.25 mm × 30 m Rtx-5 capillary column) employing *n*-dodecane as the internal standard. Photoluminescence spectra were obtained using a Perkin Elmer LS-55 fluorescence spectrometer.

3.2 Preparation of catalysts

ZIF-8 was synthesized following a previously reported method with some modifications[35]. Typically, 300 mg of $Zn(CH_3COO)_2{\cdot}2H_2O$ dissolved in 5 mL of deionized water was added to 1.12 g of 2-MIM dissolved in 6.4 mL of deionized water in a 20 mL glass vial. After shaking the glass vial for 1 min, the mixture was allowed to stand for 2 h at 25 ℃. The white product was collected by centrifugation and washed three times with deionized water and three times with acetone. The resulting precipitate was dried at 70 ℃ under vacuum for 1 h and activated under vacuum for 12 h at 130 ℃.

Pd_{PVP} nanoparticles were synthesized following a previously reported method with some modifications[24]. Typically, 210 mg of PVP (M_w ~5 5000), 120 mg of ascorbic acid, and 10 mg of KBr were dissolved in 16 mL of deionized water in a 50 mL round-bottom flask. The solution was heated to 80 ℃, and 6 mL of K_2PdCl_4 (114 mg) aqueous solution was added and the mixture maintained at 80 ℃ for 3 h. The Pd_{PVP} nanoparticles were collected by centrifugation and washed five times with acetone. Finally, the obtained Pd_{PVP} nanoparticles were dispersed in 3 mL deionized water (2 mg/mL).

Pd_{PVP}/ZIF-8 was synthesized following a previously reported method with some modifications[36]. Typically, 100 mg ZIF-8 was dispersed in acetone (1 mL), 1 mL of the Pd_{PVP} nanoparticle aqueous solution was added, and the mixture was stirred overnight. The product was collected by centrifugation, washed twice with acetone, and dried at 70 ℃ under vacuum for 1 h.

Pd/ZIF-8 was synthesized following a previously reported method with some modifications[37]. Typically, 100 mg of ZIF-8 was added to 1 mL of acetone in a 10 mL centrifuge tube and sonicated for 2 min. Subsequently, 40 μL of $Pd(NO_3)_2$ aqueous solution (50 mg Pd per mL) was added, and the mixture was stirred overnight. The product was collected by centrifugation and dried at 70 ℃ under vacuum for 1 h. The Pd/ZIF-8 was finally obtained by reduction in a 20% H_2/Ar atmosphere (50 mL/min) for 2 h at 200 ℃.

3.3 Characterizations

Mott-Schottky plot measurements were performed using a standard three-electrode system on a Zahner Zennium electrochemical workstation. Typically, 2 mg of the catalyst was added to a mixture of 2 mL ethanol and 10 μL Nafion dispersion. The mixture was then sonicated for 20 min. A 0.1 mol/L Na_2SO_4 solution was used as electrolyte. Glassy carbon coated with 30 μL of the mixed solution was used as the working electrode. A Pt plate was used as the counter electrode and an Ag/AgCl electrode as the reference electrode.

DOI: 10.52396/JUSTC-2022-0063
JUSTC, **2022**, 52(8): 5

The measurements were performed at frequencies of 500 Hz, 1000 Hz, and 1500 Hz.

The CO-DRIFT analysis was performed using a Nicolet™ iS™ 10 FTIR spectrometer equipped with an MCT detector. Typically, 25 mg of the catalyst was packed in a sample cup and sealed in an infrared (IR) reaction chamber. The sample was heated to 130 ℃ and maintained at that temperature for 0.5 h under Ar flow (25 mL/min) and 1 h under H_2/Ar flow (25 mL/min). After cooling to room temperature, background signals were collected. Then the sample was held under a heated (150 ℃) 10% CO/Ar flow (25 mL/min) for 2 h. After flushing the sample with Ar flow (25 mL/min) for 1.5 h to remove the physically adsorbed CO, the IR signal of chemically adsorbed CO was obtained.

3.4 Photocatalytic reaction

Typically, 10 mg catalyst, 80 mg K_2CO_3, 10 μL iodobenzene (0.1 mmol), 24 mg phenylboronic acid (0.2 mmol) and 2 mL DMF/water (1/1, v/v) were placed in a 140 mL optical reaction vessel. After sonication for 2 min, the suspension was purged with nitrogen for 20 min to remove the O_2. The mixture was then irradiated using an LED lamp (450 nm, 80 W) with stirring for 5 h. The conversion and yield were determined by GC analysis, using *n*-dodecane as an internal standard.

For catalysis by the physical mixture of Pd_{PVP} and ZIF-8, 100 μL of Pd_{PVP} aqueous solution and 10 mg ZIF-8 were added to 1mL of DMF and 0.9 mL deionized water while other experimental parameters were maintained constant.

For reactions with other substrates, in a typical experiment, 0.1 mmol of iodobenzene and 0.2 mmol of phenylboronic acid was added, maintaining all other experimental parameters constant.

For the scavenging experiments, *p*BQ (25 mmol/L) or MeOH (200 mmol/L) was added, maintaining all other experimental parameters constant.

For recycling experiments, the reaction solution was centrifuged at 13000 r/min for 3 min after each cycle and washed once with DMF. The catalyst was then reused for subsequent runs under standard reaction conditions.

4 Conclusions

In summary, two catalysts, Pd_{PVP}/ZIF-8 and Pd/ZIF-8, were successfully synthesized with similar Pd sizes and loading amounts. The difference in the interface between the Pd nanoparticles and the MOFs of the two catalysts induces distinct Pd electronic states. In the photocatalytic Suzuki coupling reaction, the activity of Pd/ZIF-8 outperformed that of Pd_{PVP}/ZIF-8, and both catalysts showed excellent stability. Moreover, various substrates were well tolerated in the reaction catalyzed by Pd/ZIF-8. From an analysis of the photocatalytic mechanism and the interfacial electron transfer process, the higher activity of Pd/ZIF-8 was attributed to favorable electron transfer from ZIF-8, which resembles an n-type semiconductor, to the Pd nanoparticles at the “clean” interface. This work highlights the conclusion that the regulation of interfacial electron transfer can boost the photocatalytic Suzuki coupling activity of Pd nanoparticles.

Acknowledgements

This work was supported by the National Key Research and Development Program of China (2021YFA1500400), the National Natural Science Foundation of China (21725101, 21871244, 22161142001), Collaborative Innovation Program of Hefei Science Center, CAS (2020HSC-CIP005) and the Fundamental Research Funds for the Central Universities (WK3450000007, WK2060000038).

Conflict of interest

The authors declare that they have no conflict of interest.

Biographies

Zi-Xuan Sun received his bachelor’s degree from Nankai University. He is currently a graduate student at the University of Science and Technology of China. His current research interests include metal-organic frameworks (MOFs) and photocatalytic organic reactions.

Hai-Long Jiang received his Ph.D. degree from the Fujian Institute of Research on the Structure of Matter, Chinese Academy of Sciences in 2008, and worked at AIST (Japan) as an AIST and JSPS fellow from 2008 to 2011. After postdoctoral study at Texas A&M University (USA), he joined the faculty of the University of Science and Technology of China in 2013. He has published more than 170 papers with over 31000 citations (H-index 88). His main research interest is the development of crystalline porous and nanostructured materials, combining coordination chemistry with nanoscience for the advancement of energy- and environment-related catalysis.

References

[1] Miyaura N, Suzuki, A. Stereoselective synthesis of arylated (E) -alkenes by the reaction of alk-1 -enylboranes with aryl halides in the presence of palladium catalyst. *J. C. S. Chem. Comm.*, **1979**: 866–867.

[2] Miyaura N, Yamada K, Suzuki A. A new stereospecific cross-coupling by the palladium-catalyzed reaction of 1-alkenylboranes with 1-alkenyl or 1-alkynyl halides. *Tetrahedron Lett.*, **1979**, *20* (36): 3437–3440.

[3] Buchwald S L. Cross coupling. *Acc. Chem. Res.*, **2008**, *41* (11): 1439.

[4] Wang F, Mielby J, Richter F H, et al. A polyphenylene support for Pd catalysts with exceptional catalytic activity. *Angew. Chem. Int. Ed.*, **2014**, *53* (33): 8645–8648.

[5] Sarina S, Zhu H Y, Xiao Q, et al. Viable photocatalysts under solar-spectrum irradiation: nonplasmonic metal nanoparticles. *Angew. Chem. Int. Ed.*, **2014**, *53* (11): 2935–2940.

[6] Jin Z, Xiao M D, Bao Z H, et al. A general approach to mesoporous metal oxide microspheres loaded with noble metal nanoparticles. *Angew. Chem. Int. Ed.*, **2012**, *51* (26): 6406–6410.

[7] Wang Y Q, Wang, C T, Wang L X, et al. Zeolite fixed metal nanoparticles: New perspective in catalysis. *Acc. Chem. Res.*, **2021**, *54* (11): 2579–2590.

[8] Li X H, Antonietti M. Metal nanoparticles at mesoporous N-doped carbons and carbon nitrides: functional Mott-Schottky heterojunctions for catalysis. *Chem. Soc. Rev.*, **2013**, *42* (16): 6593–6604.

[9] van Deelen T W, Hernández Mejía C, de Jong K P. Control of metal-support interactions in heterogeneous catalysts to enhance activity and selectivity. *Nat. Catal.*, **2019**, *2* (11): 955–970.

[10] Nilsson Pingel T, Jørgensen M, Yankovich A B, et al. Influence of atomic site-specific strain on catalytic activity of supported

DOI: 10.52396/JUSTC-2022-0063
JUSTC, **2022**, 52(8): 5

nanoparticles. *Nat. Commun.*, **2018**, *9* (1): 2722.
[11] Huang J, He S, Goodsell J L, et al. Manipulating atomic structures at the Au/TiO_2 interface for O_2 activation. *J. Am. Chem. Soc.*, **2020**, *142* (14): 6456–6460.
[12] Komanoya T, Kinemura T, Kita Y, et al. Electronic effect of ruthenium nanoparticles on efficient reductive amination of carbonyl compounds. *J. Am. Chem. Soc.*, **2017**, *139* (33): 11493–11499.
[13] Wang H, Wang L, Lin D, et al. Strong metal-support interactions on gold nanoparticle catalysts achieved through Le Chatelier' s principle. *Nat. Catal.*, **2021**, *4* (5): 418–424.
[14] Furukawa H, Cordova K E, O'Keeffe M, et al. The chemistry and applications of metal-organic frameworks. *Science,* **2013**, *341* (6149): 1230444.
[15] Zhou H C, Kitagawa S. Metal-organic frameworks (MOFs). *Chem. Soc. Rev.*, **2014**, *43* (16): 5415–5418.
[16] Li H, Li L B, Lin R B, et al. Porous metal-organic frameworks for gas storage and separation: Status and challenges. *EnergyChem,* **2019**, *1* (1): 100006.
[17] Yang Q H, Xu Q, Jiang H L. Metal-organic frameworks meet metal nanoparticles: synergistic effect for enhanced catalysis. *Chem. Soc. Rev.*, **2017**, *46* (15): 4774–4808.
[18] Li L Y, Li Z X, Yang W J, et al. Integration of Pd nanoparticles with engineered pore walls in MOFs for enhanced catalysis. *Chem,* **2021**, *7* (3): 686–698.
[19] Kolobov N, Goesten M G, Gascon J. Metal-organic frameworks: molecules or semiconductors in photocatalysis? *Angew. Chem. Int. Ed.,* **2021**, *60* (50): 26038–26052.
[20] Xiao J D, Han L L, Luo J, et al. Integration of plasmonic effects and schottky junctions into metal-organic framework composites: steering charge flow for enhanced visible-light photocatalysis. *Angew. Chem. Int. Ed.,* **2018**, *57* (4): 1103–1107.
[21] Xu M L, Li D D, Sun K, et al. Interfacial microenvironment modulation boosting electron transfer between metal nanoparticles and MOFs for enhanced photocatalysis. *Angew. Chem. Int. Ed.,* **2021**, *60* (30): 16372–16376.
[22] Park K S, Ni Z, Côté A P, et al. Exceptional chemical and thermal stability of zeolitic imidazolate frameworks. *Proc. Natl. Acad. Sci. U. S. A.*, **2006**, *103*: 10186–10191.
[23] Huang X C, Lin Y Y, Zhang J P, et al. Ligand-directed strategy for zeolite-type metal-organic frameworks: zinc(II) imidazolates with unusual zeolitic topologies. *Angew. Chem. Int. Ed.,* **2006**, *45* (10): 1557–1559.
[24] Li L Y, Yang W J, Yang Q H, et al. Accelerating chemo- and regioselective hydrogenation of alkynes over bimetallic nanoparticles in a metal–organic framework. *ACS Catal.,* **2020**, *10* (14): 7753–7762.
[25] Xu H Q, Hu J H, Wang D K, et al. Visible-light photoreduction of CO_2 in a metal-organic framework: boosting electron-hole separation via electron trap states. *J. Am. Chem. Soc.,* **2015**, *137* (42): 13440–13443.
[26] Pei L, Li T Z, Yuan Y J, et al. Schottky junction effect enhanced plasmonic photocatalysis by TaON@Ni NP heterostructures. *Chem. Commun.,* **2019**, *55* (78): 11754–11757.
[27] Lo W S, Chou L Y, Young A P, et al. Probing the interface between encapsulated nanoparticles and metal-organic frameworks for catalytic selectivity control. *Chem. Mater.,* **2021**, *33* (6): 1946–1953.
[28] Hayyan M, Hashim M A, AlNashef I M. Superoxide ion: Generation and chemical implications. *Chem. Rev.,* **2016**, *116* (5): 3029–3085.
[29] htarev D S, Shtareva A V, Blokh A I, et al. On the question of the optimal concentration of benzoquinone when it is used as a radical scavenger. *Appl. Phys. A,* **2017**, *123* (9): 602.
[30] Luo S Q, Ren X H, Lin H W, et al. Plasmonic photothermal catalysis for solar-to-fuel conversion: current status and prospects. *Chem. Sci,* **2021**, *12* (16): 5701–5719.
[31] Prajapati P K, Saini S, Jain S L. Nickel mediated palladium free photocatalytic Suzuki-coupling reaction under visible light irradiation. *J. Mater. Chem. A,* **2020**, *8* (10): 5246–5254.
[32] Wang Z J, Ghasimi S, Landfester K, et al. Photocatalytic Suzuki coupling reaction using conjugated microporous polymer with immobilized palladium nanoparticles under visible light. *Chem. Mater.,* **2015**, *27* (6): 1921–1924.
[33] MacQuarrie S, Horton J H, Barnes J, et al. Visual observation of redistribution and dissolution of palladium during the Suzuki-Miyaura reaction. *Angew. Chem. Int. Ed.,* **2008**, *47* (17): 3279–3282.
[34] Bai S, Jiang J, Zhang Q, et al. Steering charge kinetics in photocatalysis: intersection of materials syntheses, characterization techniques and theoretical simulations. *Chem. Soc. Rev.,* **2015**, *44*: 2893–2939.
[35] Avci C, Imaz I, Carne-Sanchez A, et al. Self-assembly of polyhedral metal-organic framework particles into three-dimensional ordered superstructures. *Nat. Chem.,* **2017**, *10* (1): 78–84.
[36] Xiao J D, Shang Q C, Xiong Y J, et al. Boosting photocatalytic hydrogen production of a metal–organic framework decorated with platinum nanoparticles: The platinum location matters. *Angew. Chem. Int. Ed.,* **2016**, *55*: 9389–9393.
[37] Liu H, Xu C Y, Li D D, et al. Photocatalytic hydrogen production coupled with selective benzylamine oxidation over MOF composites. *Angew. Chem. Int. Ed.,* **2018**, *57* (19): 5379–5383.

DOI: 10.52396/JUSTC-2022-0063
JUSTC, **2022**, 52(8): 5